Research Square

Preprints are preliminary reports that have not undergone peer review.
They should not be considered conclusive, used to inform clinical practice,
or referenced by the media as validated information.

Bacterial dysbiosis in sinonasal fungal ball: a paired 16S rRNA gene sequencing study

Pengyu Shi
Beijing Tongren Hospital
Yi Wang
Beijing Tongren Hospital
Yuan Zhang
Beijing Tongren Hospital
Ting Yang
Beijing Tongren Hospital
Jie Zhou
Beijing Tongren Hospital
Yun Zeng
Beijing Tongren Hospital
Shouxiang Dong
Beijing Tongren Hospital
Yunchuan Li
19641iyunchuan@163.com
Beijing Tongren Hospital
Hongzheng Wei
Beijing Tongren Hospital

Research Article

Keywords: Dysbiosis, Fungal ball, Microbiota, 16S, Sinusitis

Posted Date: November 1st, 2026

DOI: https://doi.org/10.21203/rs.3.rs-11004578/v1

License: This work is licensed under a Creative Commons Attribution 4.0 International License.
Read Full License

Additional Declarations: No competing interests reported.

Abstract

Purpose

Sinonasal fungal ball is usually classified as a non-invasive fungal disease. However, the bacterial changes that accompany the lesion are still not well defined. This study compared bacterial community structure and predicted functional potential between the affected sinus and the contralateral healthy side in patients with sinonasal fungal ball.

Methods

Using high-throughput 16S rRNA gene sequencing, 29 paired sinus samples were analysed, including fungal ball diseased-side samples (FBDS) and matched healthy-side samples (FBHS). The cohort included 25 maxillary sinus fungal ball pairs and 4 sphenoid sinus fungal ball pairs. Taxonomic composition, alpha diversity, beta diversity, genus-level differential abundance, co-abundance networks, and PICRUSt-predicted KEGG functional profiles were compared.

Results

FBDS and FBHS had distinct bacterial profiles. FBDS showed enrichment of Proteobacteria, Bacteroidetes and Fusobacteria, reduced alpha diversity, altered Bray-Curtis structure, and greater dispersion. Sixteen robust differential genera were identified, including FBDS-enriched *Achromobacter* and FBHS-enriched *Ochrobactrum, Desulfovibrio, Lactobacillus, Lentzea, Sphingomonas, Staphylococcus* and *Corynebacterium*. FBHS also showed a denser co-abundance network. PICRUSt predicted FBDS enrichment in lipopolysaccharide/glycan biosynthesis and translation-related pathways, whereas FBHS was linked to xenobiotic degradation and lipid metabolism. Most findings persisted in maxillary-only analysis.

Conclusion

Sinonasal fungal ball was associated with local bacterial dysbiosis on the affected side. The main features were reduced diversity, altered community composition, higher inter-individual variation, a simpler co-abundance structure, and different predicted functional potential. These findings suggest that fungal ball disease may involve localized bacterial ecological remodeling, not only fungal colonization.

INTRODUCTION

Sinonasal fungal ball is usually classified as a non-invasive form of fungal rhinosinusitis. It is often diagnosed when dense fungal material is found within a sinus cavity, most commonly in immunocompetent patients. In clinical practice, the lesion is usually treated by endoscopic surgery

(Fadda et al. 2021). The affected sinus also has impaired ventilation and drainage, mucus retention, and local inflammation. These conditions can change the bacterial ecosystem that surrounds the fungal ball (Liu et al. 2026).

The sinonasal bacterial community is part of the local mucosal environment. Studies of chronic rhinosinusitis have shown that disease states are often linked to reduced microbial diversity, expansion of dominant taxa, and altered community structure(Wagner Mackenzie et al. 2017; Cope et al. 2017). These changes do not always follow one fixed pattern, but they suggest that loss of community balance may be involved in chronic sinonasal inflammation. For fungal ball disease, culture-based studies have also reported bacterial co-infection, including Staphylococcus, Streptococcus, Enterobacter, and Pseudomonas(Wang et al. 2010; Zhang et al. 2015). More recent sequencing studies further suggest that fungal ball or fungal rhinosinusitis samples can have bacterial profiles that differ from those seen in non-fungal rhinosinusitis or healthy controls(Lu et al. 2019; Huang et al. 2023; Roh et al. 2024).

Even so, the bacterial ecology of sinonasal fungal ball remains incompletely described. Many previous studies compared unrelated patient groups or focused mainly on bacterial composition. This makes it difficult to separate lesion-related changes from host background, environmental exposure, and other between-subject differences. In addition, bacterial dysbiosis may not be limited to the rise or fall of a few genera. It may also involve changes in diversity, community dispersion, co-abundance structure, and predicted functional potential(Yang et al. 2026; Wang et al. 2025).

In this study, we analysed 29 paired sinus samples from patients with sinonasal fungal ball. Each pair included a fungal ball diseased-side sample (FBDS) and a matched healthy-side sample (FBHS). We also performed a maxillary-only sensitivity analysis to test the stability of the main findings. The aim was to determine whether the affected sinus shows local bacterial ecological remodeling and to identify the taxonomic and predicted functional features that may characterize this local microenvironment.

MATERIALS AND METHODS

Patient Recruitment and Sample Collection

This study was approved by the Ethics Committee of Beijing Tongren Hospital, Capital Medical University (approval number: MR-11-25-059116). All participants provided written informed consent. Twenty-nine adult patients with paranasal sinus fungal ball were enrolled. Patients were excluded if they had received oral antibiotics, oral corticosteroids, topical intranasal glucocorticoids within 4 weeks before surgery, or nasal irrigation within 2 weeks before surgery. Additional exclusion criteria were age under 18 years, cystic fibrosis, immunodeficiency, autoimmune disease, and primary mucociliary dysfunction.

For each patient, the CT-defined fungal ball side was classified as the diseased side, and the contralateral side was classified as the healthy side. All diagnoses were confirmed by postoperative pathology. Sinonasal swabs were collected under aseptic conditions during endoscopic sinus surgery. Healthy-side samples were obtained immediately after general anaesthesia and before any nasal

intervention. After disinfection of the nasal vestibule with iodophor, sterile swabs were placed in the middle meatus of the healthy side for at least 1 min. Diseased-side samples were collected after opening the affected sinus, with sterile swabs placed in the sinus cavity until fully infiltrated. All samples were transferred to sterile tubes and stored at -80°C until DNA extraction (Yang et al. 2026) .

DNA Extraction, PCR Amplification, and Sequencing

Total genomic DNA was extracted using the Mag-Bind Soil DNA Kit (M5635-02, OMEGA, USA) according to the manufacturer's protocol. DNA quantity and quality were assessed by NanoDrop spectrophotometry and agarose gel electrophoresis.

The V3-V4 region of the 16S rRNA gene was amplified using primers 338F (5'-ACTCCTACGGGAGGCAGCA-3') and 806R (5'-GGACTACHVGGGTWTCTAAT-3') with sample-specific 7-bp barcodes. PCR was performed in 25 μL reactions using Q5 High-Fidelity DNA Polymerase. Cycling conditions were 98°C for 2 min; 25 cycles of 98°C for 15 s, 55°C for 30 s and 72°C for 30 s; and 72°C for 5 min. Amplicons were purified, quantified, pooled in equal amounts and sequenced on the Illumina MiSeq platform using paired-end 2 x 300 bp reads.

Sequence Processing and Statistical Analysis

Sequencing data were processed using QIIME v1.8.0 (Caporaso et al. 2010). Reads with exact barcode matches were assigned to samples. Low-quality reads were removed if they were shorter than 150 bp, had an average Phred score below 20, contained ambiguous bases, or contained homopolymer repeats longer than 8 bp. Paired-end reads were assembled using FLASH (Magoc and Salzberg 2011). After chimera removal, high-quality sequences were clustered into operational taxonomic units (OTUs) at 97% sequence identity using UCLUST(Edgar 2010). Representative sequences were assigned taxonomy against the Greengenes database(DeSantis et al. 2006). OTUs accounting for less than 0.001% of total sequences were removed. To reduce differences in sequencing depth, an averaged rarefied OTU table was generated from 100 resampled OTU tables at 90% of the minimum sequencing depth.

Taxonomic composition was summarized at different levels, and relative abundance was calculated as a percentage. Alpha diversity was assessed using Chao1, ACE, Shannon diversity, Simpson_1D, inverse Simpson, and Good's coverage indices. Beta diversity was evaluated using Bray-Curtis distance, and principal coordinates analysis (PCoA) was used for visualization. Pair-adjusted PERMANOVA was used to test overall community differences, and PERMDISP was used to assess differences in within-group dispersion by comparing distances to group centroids.

Paired or unpaired group differences were tested using the Wilcoxon signed-rank test or Mann-Whitney U test, as appropriate. Multiple testing was corrected using the Benjamini-Hochberg false discovery rate (FDR) method. Genus-level differential abundance was assessed after filtering low-abundance and low-

prevalence genera. Candidate differential genera were defined by statistical significance, consistent direction of change, and a predefined effect-size threshold.

For network analysis, dominant genera were selected by mean relative abundance and prevalence. Pairwise Spearman correlations were calculated within each group, and only correlations passing the correlation and FDR thresholds were retained. These networks were interpreted as co-abundance patterns, not as evidence of direct microbial interactions(Langille et al. 2013).

Bacterial functional potential was predicted from 16S rRNA profiles using PICRUSt and annotated against KEGG(Kanehisa et al. 2021). KEGG level 2 categories were used as broad functional classes, and KEGG level 3 categories were used as more specific pathways. Predicted functional profiles were normalized within each sample and converted to relative abundance percentages. Differences in predicted KEGG L2 and L3 functional potential were tested using the Wilcoxon signed-rank test with Benjamini-Hochberg FDR correction. Associations between candidate genera and KEGG pathways were explored using Spearman correlation analysis.

RESULTS

Study population

Twenty-nine patients with sinonasal fungal ball were included, comprising 6 males and 23 females. Each patient provided one fungal ball diseased-side sample (FBDS) and one matched contralateral healthy-side sample (FBHS). The cohort included 25 maxillary sinus fungal ball pairs and 4 sphenoid sinus fungal ball pairs. Demographic and clinical characteristics are summarised in Table 1.

Table 1
Patient characteristics

Characteristic	Value
Female, n (%)	23(79)
Age (years), mean ± SD	52.7 ± 13.6
Course (months), median(IQR)	10(3–48)*
Diseased sinus site, n (%)	
Maxillary sinus	25 (86.2)
Sphenoid sinus	4 (13.8)
Symptom, n (%)*	
Nasal obstruction	16(69)
Nasal discharge	14(61)
Headache	11(48)
Epistaxis/bloody discharge	6(26)
Postnasal drip	5(22)
Facial discomfort	4(17)
Sneezing	3(13)
Nasal odor	2(9)
Vision loss	1(4)
Dizziness	1(4)

*IQR, interquartile range. * 23 patients had clinical symptoms (the other 6 cases were found by CT).*

Taxonomic Composition

After quality control, sequences were assigned to taxonomic units at the highest available similarity level. Taxonomic annotation identified 30 phyla, 81 classes, 132 orders, 188 families, 321 genera, and 183 species-level taxa.

At the phylum level, FBDS was mainly composed of *Proteobacteria*, *Firmicutes*, *Bacteroidetes*, *Actinobacteria*, and *Fusobacteria*, with mean relative abundances of 46.99%, 27.50%, 14.53%, 5.19%, and 3.07%, respectively. FBHS was dominated by *Proteobacteria*, *Firmicutes*, *Actinobacteria*, *Bacteroidetes*, and *Chloroflexi*, with mean relative abundances of 37.40%, 35.84%, 12.61%, 8.80%, and 1.17%. (Fig. 1A)

At the genus level, the selected-genera plot showed compositional differences between FBDS and FBHS (Fig. 1B,1C). In this descriptive plot, *Haemophilus, Neisseria, Streptococcus, Unclassified_Planococcaceae, Capnocytophaga, Fusobacterium, Pseudomonas, Eikenella*, and *[Prevotella]* showed higher mean relative abundances in FBDS, whereas *Unclassified_Ruminococcaceae, Ochrobactrum, Unclassified_S24-7, Desulfovibrio, Lactobacillus*, and *Lentzea* showed higher mean relative abundances in FBHS. These selected genera were used to visualize genus-level compositional patterns and should be distinguished from the high-confidence candidate differential genera identified by the paired statistical screening. Site-stratified analysis showed different genus-level profiles between maxillary and sphenoid FBDS samples, but the sphenoid subgroup was small and was therefore interpreted as exploratory.

Alpha and Beta Diversity

FBHS showed higher alpha diversity than FBDS across the paired cohort. Chao1 richness and Shannon diversity were significantly higher in FBHS, and additional diversity metrics, including ACE, Simpson_1D, and inverse Simpson, supported the same overall pattern (Table 2). This pattern was retained in the maxillary-only sensitivity analysis after exclusion of the four sphenoid pairs.

Table 2
Alpha-diversity indices

Overall 29 pairs						
Index	FBDS (mean ± SD)	FBHS (mean ± SD)	Test statistic	P value	FDR	Statistical test
Chao1	1466.09 ± 817.45	2525.70 ± 764.89	W = 28.0	< 0.001	< 0.001	Paired Wilcoxon
ACE	1489.04 ± 849.10	2538.69 ± 791.41	W = 28.0	< 0.001	< 0.001	
Shannon	4.10 ± 1.01	5.63 ± 0.87	W = 38.0	< 0.001	< 0.001	
Simpson (1-D)	0.91 ± 0.10	0.96 ± 0.05	W = 85.0	0.003	0.003	signed-rank test
Inverse Simpson	26.17 ± 30.73	69.11 ± 42.84	W = 61.0	< 0.001	< 0.001	
Good's coverage	0.98 ± 0.01	0.97 ± 0.01	W = 35.5	< 0.001	< 0.001	
Maxillary sinus 25 pairs						
Index	FBDS (mean ± SD)	FBHS (mean ± SD)	Test statistic	P value	FDR	Statistical test
Chao1	1457.94 ± 874.95	2603.17 ± 791.10	W = 19.0	< 0.001	< 0.001	Paired Wilcoxon
ACE	1484.60 ± 909.43	2609.18 ± 828.28	W = 20.0	< 0.001	< 0.001	
Shannon	4.07 ± 1.07	5.71 ± 0.87	W = 26.0	< 0.001	< 0.001	
Simpson (1-D)	0.90 ± 0.10	0.97 ± 0.05	W = 56.0	0.003	0.003	signed-rank test
Inverse Simpson	27.20 ± 32.68	74.64 ± 42.82	W = 41.0	< 0.001	< 0.001	
Good's coverage	0.98 ± 0.01	0.97 ± 0.01	W = 26.0	< 0.001	< 0.001	
FBDS site subgroup comparison						
Index	Maxillary sinus	Sphenoid sinus	Test	P	FDR	Statistical test

Notes: Values are presented as mean±SD. P values were adjusted by the Benjamini–Hochberg false discovery rate FDR method.

Overall 29 pairs						
	FBDS (mean ± SD)	FBDS (mean ± SD)	statistic	value		
Chao1	1457.94 ± 874.95	1517.01 ± 329.37	U = 45.0	0.784	0.784	Mann–Whitney
ACE	1484.60 ± 909.43	1516.81 ± 333.83	U = 44.0	0.737	0.784	
Shannon	4.07 ± 1.07	4.25 ± 0.57	U = 44.0	0.737	0.784	
Simpson (1-D)	0.90 ± 0.10	0.93 ± 0.05	U = 55.0	0.784	0.784	U test
Inverse Simpson	27.20 ± 32.68	19.73 ± 14.30	U = 55.0	0.784	0.784	
Good's coverage	0.98 ± 0.01	0.98 ± 0.01	U = 55.0	0.784	0.784	

Notes: Values are presented as mean±SD. P values were adjusted by the Benjamini–Hochberg false discovery rate FDR method.

Bray-Curtis beta diversity showed different overall community structures between FBDS and FBHS (Fig. 2A). Principal coordinates analysis showed partial separation between groups, and pair-adjusted PERMANOVA confirmed a significant group difference (Pseudo-F = 4.714, R2 = 0.066, P < 0.001). FBDS also showed greater within-group dispersion than FBHS, with a higher mean distance to the group centroid (0.658 vs. 0.563; PERMDISP: F = 42.120, P < 0.001; paired Wilcoxon test: P = 2.84 x 10^-6).

The maxillary-only sensitivity analysis produced similar results. Community structure still differed between FBDS and FBHS (PERMANOVA: Pseudo-F = 4.815, R2 = 0.078, P < 0.001), and dispersion remained higher in FBDS (PERMDISP: F = 40.462, P < 0.001; paired Wilcoxon test: P = 1.23 x 10^-5). The paired FBDS-FBHS Bray-Curtis distance was high in both the overall and maxillary-only analyses, with median values of 0.868 and 0.905, respectively (Fig. 2B,2C).

Candidate differential genera and co-abundance networks

Genus-level differential abundance analysis was performed in all 29 paired samples and repeated in the 25 maxillary pairs. Candidate differential genera were required to meet three criteria: FDR < 0.05 in both analyses, the same direction of change in both analyses and an absolute mean relative abundance difference of at least 0.5 percentage points in both comparisons. Among 162 clearly annotated genera included in both analyses, 87 showed significant and directionally consistent differences between FBDS and FBHS. After applying the effect-size filter, 16 high-confidence candidate differential genera remained (Fig. 3A). *Achromobacter* was enriched in FBDS, whereas *Ochrobactrum, Desulfovibrio, Lactobacillus, Lentzea, Cryocola, Cupriavidus, Methylobacterium, Delftia, Thermus, Sphingomonas, Propionibacterium, Amycolatopsis, Staphylococcus, Anoxybacillus* and *Corynebacterium* were enriched in FBHS. No genus

remained significant after FDR correction in the exploratory comparison between maxillary and sphenoid FBDS samples. Spearman co-abundance networks were then constructed separately for FBDS and FBHS using the top 50 dominant genera detected in at least 10% of samples, retaining only correlations with |rho| > 0.6 and FDR < 0.05 (Fig. 3B,3C). The FBDS network contained 45 connected nodes and 189 significant edges, all of which were positive, with a network density of 0.154. Highly connected genera in FBDS included *Cupriavidus, Ochrobactrum, Thermus, Bacillus* and *Sphingomonas*. The FBHS network contained 44 connected nodes and 281 significant edges, including 248 positive and 33 negative correlations, with a higher network density of 0.229. Highly connected genera in FBHS included *Streptomyces, Methylobacterium, Amycolatopsis, Delftia* and *Bacillus*.

Predicted Functional Potential

PICRUSt-based KEGG prediction identified differences in predicted functional potential between FBDS and FBHS. At KEGG level 2, 22 of 38 tested categories differed significantly between groups. Eleven categories were higher in FBDS and 11 were higher in FBHS. FBDS-enriched categories mainly involved glycan biosynthesis and metabolism, replication and repair, translation, folding, sorting and degradation, and nucleotide metabolism. FBHS-enriched categories mainly involved membrane transport, xenobiotic biodegradation and metabolism, carbohydrate metabolism, amino acid metabolism and cell motility (Fig. 4A).

At KEGG level 3, 86 of 229 tested pathways differed significantly between groups. Forty-two pathways were higher in FBDS and 44 were higher in FBHS. FBDS-enriched pathways were mainly related to lipopolysaccharide biosynthesis, glycosylation, protein folding, translation and ribosome biogenesis. FBHS-enriched pathways were mainly related to xenobiotic degradation and lipid-associated metabolism. These differences were largely retained in the maxillary-only sensitivity analysis, with 18 level 2 categories and 72 level 3 pathways showing consistent significance and direction (Fig. 4B).

Exploratory correlation analysis identified 15 significant associations between paired genus-level differences and paired KEGG level 3 pathway differences after FDR correction. Representative associations included positive correlations of *Cupriavidus, Lentzea* and *Lactobacillus* with nitrotoluene degradation, and negative correlations of *Lactobacillus* and *Desulfovibrio* with lipoic acid metabolism (Fig. 4C).

DISCUSSION

Advances in high-throughput sequencing have moved sinonasal microbiome research beyond the limited range of taxa detectable by conventional culture, enabling community-level assessment of local bacterial ecology(Bassiouni et al. 2015; Hauser et al. 2015). Previous studies have suggested that the sinonasal bacterial microbiota in patients with fungal rhinosinusitis differs from that in healthy individuals or patients with non-fungal rhinosinusitis. However, most studies have used unpaired designs and are therefore susceptible to confounding by age, comorbidities, medication history, living environment, and

other host-related factors (Dellière et al. 2021; Lu et al. 2019; Roh et al. 2024). In the present study, we used a self-controlled paired design comparing fungal ball-affected sinuses with contralateral unaffected sinuses from the same patients, which reduced inter-individual confounding and allowed a more focused assessment of lesion-associated microbial alterations. Based on this design, our findings suggest that sinus fungal ball disease is not merely characterized by the presence of fungal aggregates or debris within the sinus cavity, but is also accompanied by changes in the local bacterial community. Alpha diversity analysis showed reduced microbial richness and evenness in the affected sinuses, whereas beta diversity analysis revealed distinct overall community structures between affected and unaffected sinuses, with greater dispersion among FBDS samples. These findings highlight the heterogeneity and remodeling characteristics of the microbial microenvironment associated with sinus fungal ball disease. The co-occurrence network analysis further supported this interpretation. The contralateral unaffected sinuses showed a denser and more connected bacterial network, with both positive and negative correlations among genera, suggesting a relatively stable ecological structure in which taxa may coexist, compete, or occupy distinct niches. In contrast, the fungal ball-affected sinuses showed a sparser network, and the remaining associations were mainly positive. Although correlation-based networks cannot prove direct microbial interactions or demonstrate loss of pre-existing ecological relationships, this pattern, together with reduced alpha diversity and increased beta-diversity dispersion, suggests a simplified community structure and potentially weakened inter-taxon constraints in the affected sinus. Impaired sinus ventilation and drainage, mucus retention, local inflammation, and long-term fungal-bacterial coexistence may alter local oxygen tension, nutrient availability, and mucosal immune status, thereby creating conditions that favor selective expansion of certain bacterial genera (Ramakrishnan et al. 2017; Proctor and Relman 2017).

At the genus level, the selected-genera composition plot showed higher mean relative abundances of several FBDS-associated genera, including *Haemophilus, Neisseria, Streptococcus, Capnocytophaga, Fusobacterium, Pseudomonas, Eikenella*, and *[Prevotella]*. In contrast, the stricter paired differential-abundance framework identified *Achromobacter* as the only high-confidence FBDS-enriched candidate genus, whereas multiple candidate genera were enriched in FBHS. Importantly, increased relative abundance does not necessarily indicate an increase in absolute bacterial load, nor does it establish a genus as a pathogen. It may reflect preferential growth under the altered microenvironment of the affected sinus, or a passive increase in proportion caused by depletion of other taxa. These genera should therefore be interpreted as indicators of local microecological alteration rather than as single causal agents. *Haemophilus* illustrates this point. Previous studies have reported increased detection and relative abundance of *Haemophilus* in fungal rhinosinusitis samples, and potential interactions between *Haemophilus* influenzae and Aspergillus fumigatus have also been proposed (Shi et al. 2023; Yang et al. 2026; Lu et al. 2019). In our study, *Haemophilus* was also relatively abundant in FBDS, suggesting marked expansion in a subset of affected sinuses. However, it did not form significant network links under the predefined threshold, and the affected-side communities showed high dispersion. Thus, *Haemophilus* should not be interpreted as a core pathogen driving sinus fungal ball formation, but rather as one of the dominant colonizers emerging in a dysbiotic microbial state. Unlike

Haemophilus, Achromobacter was not the most abundant genus in FBDS, but it was a stably enriched candidate differential genus under our screening framework. This suggests a relatively robust statistical association between *Achromobacter* and the affected-side microbial state. Previous microbiome studies of fungal rhinosinusitis have also reported detection of *Achromobacter* only in middle meatus samples from patients with fungal rhinosinusitis (Lu et al. 2019). Positive sinus cultures for Achromobacter have also been reported in refractory chronic rhinosinusitis (Dobson et al. 2018), and other studies have linked this genus to multidrug resistance, biofilm formation, in-host adaptation, secretion systems, and competition with other pathogens (Bador et al. 2013; Cameron et al. 2019; Khademi et al. 2021; Gabrielaite et al. 2021). In the present study, however, *Achromobacte*r is best interpreted as a candidate marker of lesion-associated microecological shift rather than as a proven causal taxon. By contrast, FBHS was enriched for a broader set of high-confidence candidate differential genera, including *Ochrobactrum, Desulfovibrio, Lactobacillus, Lentzea*, and *Cupriavidus*. These genera showed consistent directions in both the overall analysis and the maxillary-only sensitivity analysis, suggesting a more stable association with the unaffected sinus microbial state.

PICRUSt-based functional prediction further suggested that FBHS-associated genera were more closely linked to xenobiotic and aromatic compound degradation, bile acid and lipid-related metabolism, and diverse substrate-utilization pathways, indicating a more functionally diverse microbial ecosystem in the unaffected sinus. In FBDS, PICRUSt prediction showed higher functional potential for lipopolysaccharide biosynthesis, glycosyltransferases, glycan biosynthesis, translation, ribosome biogenesis, and chaperones and folding catalysts. These findings suggest that the affected-side microbiota may be functionally biased toward cell wall and bacterial surface remodeling, protein synthesis, and environmental stress adaptation (Yang et al. 2026; Njenga et al. 2023). The higher predicted potential for lipopolysaccharide biosynthesis is consistent with the increased relative abundance of Proteobacteria in FBDS and may provide a plausible link between bacterial dysbiosis and local mucosal inflammation (Bertani and Ruiz 2018). Lipopolysaccharide is a major component of the outer membrane of Gram-negative bacteria and can be recognized by innate immune pathways, particularly those involving TLR4 (Cho et al. 2014; Poltorak et al. 1998). Changes in glycosyltransferase and glycan-related pathways may also reflect remodeling of bacterial surface structures, extracellular polysaccharides, or cell wall glycoconjugates, which could facilitate bacterial persistence in a mucus-retentive, poorly drained, chronically inflamed sinus environment (Messner et al. 2013; Whitfield et al. 2015; Winstel et al. 2015; Vanderpool and Rumbaugh 2023). In addition, the higher predicted potential for translation, ribosome biogenesis, and chaperone-related pathways suggests that the affected-side microbiota may be skewed toward active growth, protein synthesis, and enhanced stress tolerance (Scott and Hwa 2011; Lund 2001). Conversely, FBHS-enriched genera were negatively correlated with several FBDS-dominant pathways, including ribosome biogenesis and translation-related proteins. Overall, the affected sinus microbiota appears to shift from a more metabolically diverse and ecologically balanced state toward a dysbiotic state characterized by bacterial surface modification, Gram-negative outer-membrane biosynthesis, increased protein synthesis, and stress adaptation.

Several limitations should be noted. First, the sphenoid sinus subgroup was small, and site-specific findings should therefore be considered exploratory. Second, 16S rRNA gene sequencing has limited taxonomic resolution and cannot reliably distinguish strain-level differences. Third, relative abundance data cannot determine whether an increased proportion of a genus reflects true absolute expansion or passive enrichment due to depletion of other taxa. Fourth, PICRUSt-based functional prediction is an indirect inference and requires validation by shotgun metagenomics, metatranscriptomics, targeted bacterial quantification, metabolomics, and host inflammatory marker analysis. Finally, because this was a cross-sectional study, we cannot determine whether bacterial dysbiosis preceded fungal ball formation, developed secondarily after lesion formation, or progressed in parallel with the disease. Nevertheless, the maxillary-only sensitivity analysis yielded consistent results, indicating that the main findings were not driven by the smaller sphenoid sinus subgroup.

The unaffected sinus maintained a more diverse bacterial community with tighter inter-taxon associations and a more balanced distribution of predicted metabolic functions. In contrast, the fungal ball-affected sinus showed reduced microbial diversity, altered taxonomic composition, greater inter-individual variability, simplified inter-taxon associations, and increased predicted functional potential related to lipopolysaccharide biosynthesis, glycosylation, protein translation, and protein folding. Together, these findings suggest that sinus fungal ball disease is closely associated with local bacterial microecological remodeling.

Declarations

ACKNOWLEDGEMENTS

We thank all the patients, and teachers who made contributions to the data collection.

AUTHORS' CONTRIBUTIONS

All authors participated in the work, and the authors' contributions are as follows: J.Z., S.D., T.Y, Y.Z, and Y.W. performed protocol development, patient enrolment, data collection, and verification. P.S and H.W. conducted data analysis and drafted the initial manuscript. Y.L. and Y.Z. provided critical input on study design and revised the manuscript. All authors participated in scientific discussions and approved the final version.

FUNDING

The authors received research grants from Beijing Natural Science Foundation of China (approval number: 7222026).

DECLARATIONS

Ethics approval and consent to participate

The study was approved by the ethics committee of Beijing Tongren Hospital, Capital Medical University. An informed consent form was signed by all participants and our study was performed in accordance with the Declaration of Helsinki. Clinical trial number: ChiCTR2500108224.

Competing interests

The authors declare no competing interests.

Consent for publication

Not applicable.

AVAILABILITY OF DATA AND MATERIALS

The raw 16S rRNA gene sequencing datasets generated during the current study are available in the NCBI Sequence Read Archive (SRA) under BioProject accession number PRJNA1529700: https://www.ncbi.nlm.nih.gov/bioproject/PRJNA1529700.

References

1. Fadda GL, Allevi F, Rosso C, Martino F, Pipolo C, Cavallo G, et al. (2021) Treatment of paranasal sinus fungus ball: a systematic review and meta-analysis. Ann Otol Rhinol Laryngol 130:1302–1310. https://doi.org/10.1177/00034894211002431
2. Liu C, Yang T, Shi P, Zeng Y, Wang Y, Li Y, et al. (2026) Analysis of sinus inflammation associated with maxillary sinus fungal ball based on CT imaging. Ear Nose Throat J 105:NP201–NP206. https://doi.org/10.1177/01455613231185044
3. Wagner Mackenzie B, Waite DW, Hoggard M, Douglas RG, Taylor MW, Biswas K (2017) Bacterial community collapse: a meta-analysis of the sinonasal microbiota in chronic rhinosinusitis. Environ Microbiol 19:381–392. https://doi.org/10.1111/1462-2920.13632
4. Cope EK, Goldberg AN, Pletcher SD, Lynch SV (2017) Compositionally and functionally distinct sinus microbiota in chronic rhinosinusitis patients have immunological and clinically divergent consequences. Microbiome 5:53. https://doi.org/10.1186/s40168-017-0266-6
5. Wang JH, Lee BJ, Jang YJ (2010) Bacterial coinfection and antimicrobial resistance in patients with paranasal sinus fungus balls. Ann Otol Rhinol Laryngol 119:406–411. https://doi.org/10.1177/000348941011900608
6. Zhang J, Li Y, Lu X, Wang X, Zang H, Wang T, et al. (2015) Analysis of fungal ball rhinosinusitis by culturing fungal clumps under endoscopic surgery. Int J Clin Exp Med 8:5925–5930.
7. Lu YT, Wang SH, Liou ML, Shen TA, Lu YC, Hsin CH, et al. (2019) Microbiota dysbiosis in fungal rhinosinusitis. J Clin Med 8:1973. https://doi.org/10.3390/jcm8111973
8. Huang YW, Wang WH, Lan MY (2023) Analysing sinonasal microbiota of fungal rhinosinusitis by next-generation sequencing. Clin Otolaryngol 48:313–320. https://doi.org/10.1111/coa.13980

9. Roh D, Shin JH, Kim SW, Kim SW, Kim BG, Cho JH, et al. (2024) Sinonasal microbiome and inflammatory profiles in fungal ball and chronic rhinosinusitis. Auris Nasus Larynx 51:242–250. https://doi.org/10.1016/j.anl.2023.11.003
10. Yang T, Wang Y, Zhang Y, Liu C, Zeng Y, Shi P, et al. (2026) Haemophilus influenzae dominance in fungal ball microbiome revealed through multi-niche metagenomic sequencing. BMC Microbiol 26:15. https://doi.org/10.1186/s12866-025-04546-8
11. Wang Y, Wei H, Yang T, Liu C, Shi P, Zhou J, et al. (2025) Metabolomics-based characterization of fungal ball sinusitis. Ear Nose Throat J. Advance online publication. https://doi.org/10.1177/01455613251361235
12. Caporaso JG, Kuczynski J, Stombaugh J, Bittinger K, Bushman FD, Costello EK, et al. (2010) QIIME allows analysis of high-throughput community sequencing data. Nat Methods 7:335–336. https://doi.org/10.1038/nmeth.f.303
13. Magoč T, Salzberg SL (2011) FLASH: fast length adjustment of short reads to improve genome assemblies. Bioinformatics 27:2957–2963. https://doi.org/10.1093/bioinformatics/btr507
14. Edgar RC (2010) Search and clustering orders of magnitude faster than BLAST. Bioinformatics 26:2460–2461. https://doi.org/10.1093/bioinformatics/btq461
15. DeSantis TZ, Hugenholtz P, Larsen N, Rojas M, Brodie EL, Keller K, et al. (2006) Greengenes, a chimera-checked 16S rRNA gene database and workbench compatible with ARB. Appl Environ Microbiol 72:5069–5072. https://doi.org/10.1128/AEM.03006-05
16. Langille MGI, Zaneveld J, Caporaso JG, McDonald D, Knights D, Reyes JA, et al. (2013) Predictive functional profiling of microbial communities using 16S rRNA marker gene sequences. Nat Biotechnol 31:814–821. https://doi.org/10.1038/nbt.2676
17. Kanehisa M, Furumichi M, Sato Y, Ishiguro-Watanabe M, Tanabe M (2021) KEGG: integrating viruses and cellular organisms. Nucleic Acids Res 49:D545–D551. https://doi.org/10.1093/nar/gkaa970
18. Bassiouni A, Cleland EJ, Psaltis AJ, Vreugde S, Wormald PJ (2015) Sinonasal microbiome sampling: a comparison of techniques. PLoS One 10:e0123216. https://doi.org/10.1371/journal.pone.0123216
19. Hauser LJ, Feazel LM, Ir D, Fang R, Wagner BD, Robertson CE, et al. (2015) Sinus culture poorly predicts resident microbiota. Int Forum Allergy Rhinol 5:3–9. https://doi.org/10.1002/alr.21428
20. Dellière S, Dannaoui E, Fieux M, Bonfils P, Gricourt G, Demontant V, et al. (2021) Analysis of microbiota and mycobiota in fungal ball rhinosinusitis: specific interaction between Aspergillus fumigatus and Haemophilus influenza? J Fungi (Basel) 7:550. https://doi.org/10.3390/jof7070550
21. Ramakrishnan VR, Gitomer S, Kofonow JM, Robertson CE, Frank DN (2017) Investigation of sinonasal microbiome spatial organization in chronic rhinosinusitis. Int Forum Allergy Rhinol 7:16–23. https://doi.org/10.1002/alr.21854
22. Proctor DM, Relman DA (2017) The landscape ecology and microbiota of the human nose, mouth, and throat. Cell Host Microbe 21:421–432. https://doi.org/10.1016/j.chom.2017.03.011
23. Shi P, Wei H, Liu X, Dong S, He S, Zeng Y, et al. (2023) The nasal bacteria microbiome comparison among fungal ball sinusitis, chronic sinusitis with polyps. Indian J Microbiol 63:120–128.

https://doi.org/10.1007/s12088-023-01062-z

24. Dobson BC, Bernard SH, Varadarajan VV, Wang GP, Justice JM (2018) The role of Achromobacter xylosoxidans positive sinus cultures in patients with refractory chronic rhinosinusitis. Otolaryngol Online J 8:172.
25. Bador J, Amoureux L, Blanc E, Neuwirth C (2013) Innate aminoglycoside resistance of Achromobacter xylosoxidans is due to AxyXY-OprZ, an RND-type multidrug efflux pump. Antimicrob Agents Chemother 57:603–605. https://doi.org/10.1128/AAC.01243-12
26. Cameron LC, Bonis B, Phan CQ, Kent LA, Lee AK, Hunter RC (2019) A putative enoyl-CoA hydratase contributes to biofilm formation and the antibiotic tolerance of Achromobacter xylosoxidans. NPJ Biofilms Microbiomes 5:20. https://doi.org/10.1038/s41522-019-0093-6
27. Khademi SMH, Gabrielaite M, Paulsson M, Knulst M, Touriki E, Marvig RL, et al. (2021) Genomic and phenotypic evolution of Achromobacter xylosoxidans during chronic airway infections of patients with cystic fibrosis. mSystems 6:e00523-21. https://doi.org/10.1128/mSystems.00523-21
28. Gabrielaite M, Nielsen FC, Johansen HK, Marvig RL (2021) Achromobacter spp. genetic adaptation in cystic fibrosis. Microb Genom 7:000582. https://doi.org/10.1099/mgen.0.000582
29. Njenga R, Boele J, Öztürk Y, Koch HG (2023) Coping with stress: how bacteria fine-tune protein synthesis and protein transport. J Biol Chem 299:105163. https://doi.org/10.1016/j.jbc.2023.105163
30. Bertani B, Ruiz N (2018) Function and biogenesis of lipopolysaccharides. EcoSal Plus 8:ESP-0001-2018. https://doi.org/10.1128/ecosalplus.ESP-0001-2018
31. Cho JS, Kang JH, Um JY, Han IH, Park IH, Lee HM (2014) Lipopolysaccharide induces pro-inflammatory cytokines and MMP production via TLR4 in nasal polyp-derived fibroblast and organ culture. PLoS One 9:e90683. https://doi.org/10.1371/journal.pone.0090683
32. Poltorak A, He X, Smirnova I, Liu MY, Van Huffel C, Du X, et al. (1998) Defective LPS signaling in C3H/HeJ and C57BL/10ScCr mice: mutations in Tlr4 gene. Science 282:2085–2088. https://doi.org/10.1126/science.282.5396.2085
33. Messner P, Schäffer C, Kosma P (2013) Bacterial cell-envelope glycoconjugates. Adv Carbohydr Chem Biochem 69:209–272. https://doi.org/10.1016/B978-0-12-408093-5.00006-X
34. Whitfield GB, Marmont LS, Howell PL (2015) Enzymatic modifications of exopolysaccharides enhance bacterial persistence. Front Microbiol 6:471. https://doi.org/10.3389/fmicb.2015.00471
35. Winstel V, Kühner P, Salomon F, Larsen J, Skov R, Hoffmann W, et al. (2015) Wall teichoic acid glycosylation governs Staphylococcus aureus nasal colonization. mBio 6:e00632-15. https://doi.org/10.1128/mBio.00632-15
36. Vanderpool EJ, Rumbaugh KP (2023) Host-microbe interactions in chronic rhinosinusitis biofilms and models for investigation. Biofilm 6:100160. https://doi.org/10.1016/j.bioflm.2023.100160
37. Scott M, Hwa T (2011) Bacterial growth laws and their applications. Curr Opin Biotechnol 22:559–565. https://doi.org/10.1016/j.copbio.2011.04.014

38. Lund PA (2001) Microbial molecular chaperones. Adv Microb Physiol 44:93–140. https://doi.org/10.1016/S0065-2911(01)44012-4

Figures

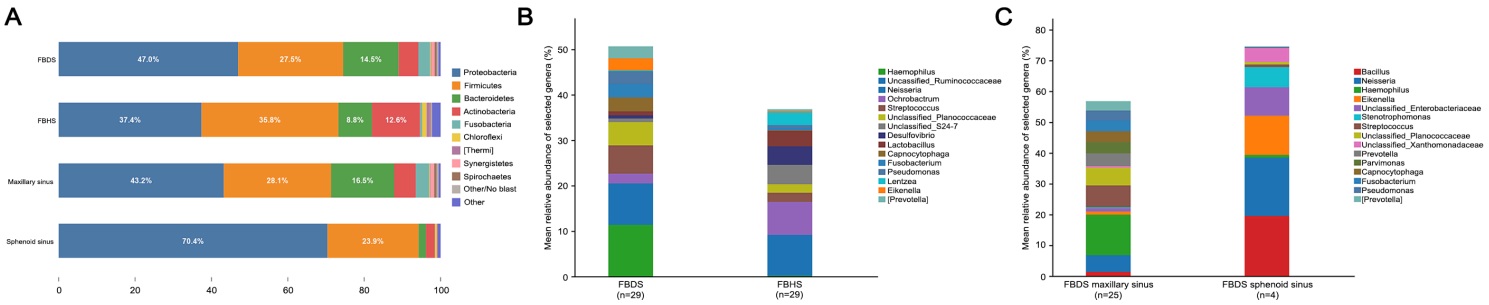


Figure 1

Taxonomic composition of bacterial communities in FBDS, FBHS, and FBDS different subgroups (A) Phylum-level community composition is shown as stacked horizontal bars representing mean relative abundance (%) in FBDS samples (n = 29), matched FBHS samples (n = 29), and FBDS samples stratified by sinus site, including maxillary sinus fungal ball (n = 25) and sphenoid sinus fungal ball (n = 4). (B) Genus-level composition of selected genera is shown for FBDS versus FBHS (n=29). (C) FBDS samples stratified by maxillary and sphenoid sinus involvement. Bars represent the summed mean relative abundance of displayed selected genera, not the complete genus-level community.

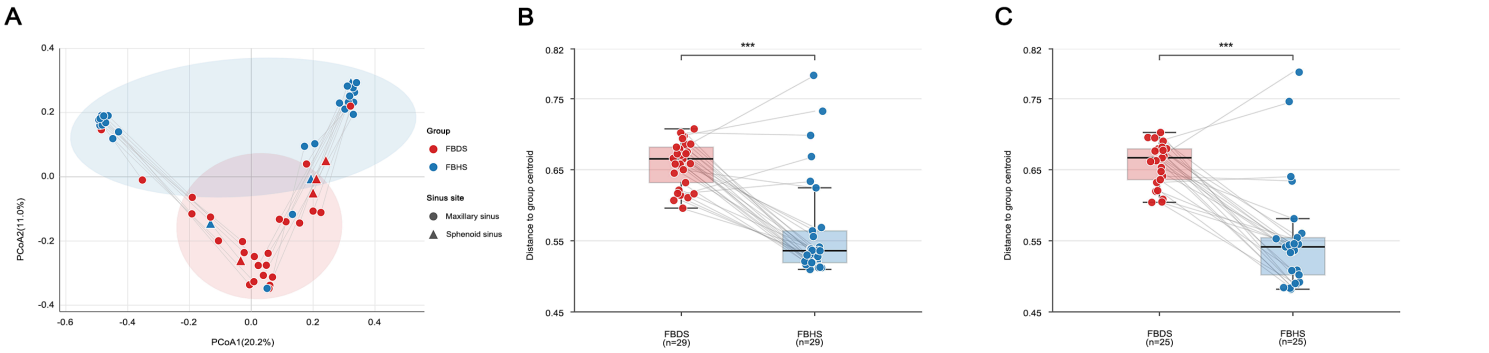


Figure 2

Bray-Curtis beta diversity and within-group dispersion of paired FBDS and FBHS samples. (A) Principal coordinates analysis (PCoA) based on Bray-Curtis dissimilarity. Points represent individual sinus samples, colours indicate sample group, and shapes indicate sinus site. Grey lines connect paired FBDS and FBHS samples from the same patient. Shaded ellipses indicate group-level distributions in ordination space. (B) Boxplots showing the distance of each sample to its group centroid in the overall paired cohort. Individual points represent samples, and grey lines connect paired samples from the

same patient. (C) Cohort analysis limited to maxillary sinus with exclusion of sphenoid sinus. Statistical significance is indicated by asterisks after false discovery rate correction. ***FDR < 0.001.

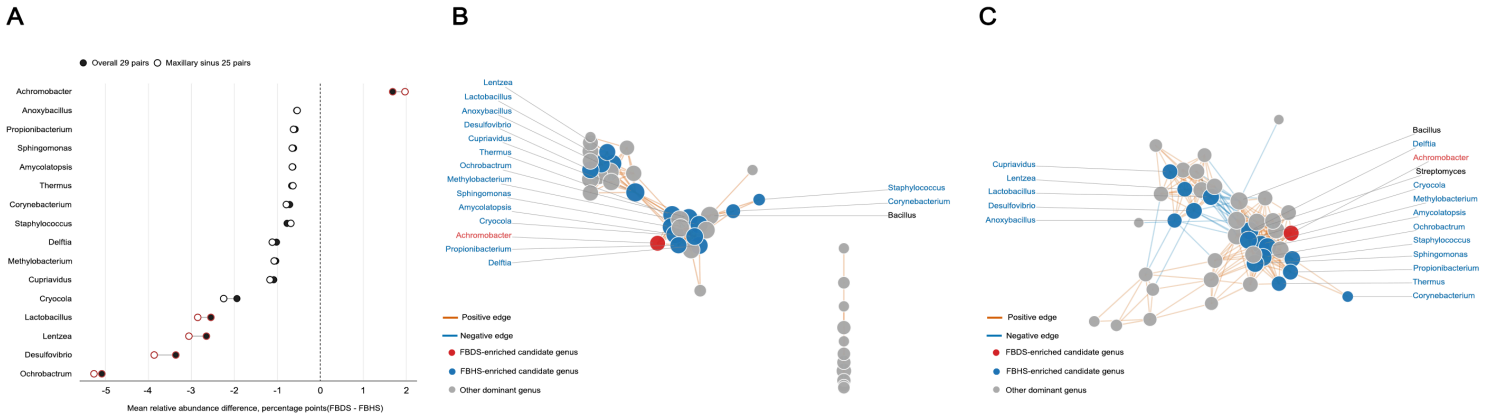


Figure 3

Candidate differential genera and genus-level Spearman co-abundance networks in paired FBDS and FBHS samples. (A) Mean relative abundance differences of candidate differential genera between FBDS and FBHS. Values are shown as percentage-point differences calculated as FBDS minus FBHS; positive values indicate higher relative abundance in FBDS, whereas negative values indicate higher relative abundance in FBHS. Filled circles represent the overall 29-pair analysis, and open circles represent the maxillary-only 25-pair analysis. Red-outlined circles indicate representative candidate genera highlighted in the manuscript text. The vertical dashed line indicates no difference between groups. (B) Spearman co-abundance networks constructed separately for dominant genera in FBDS. The 50 most abundant genera were used as input nodes. Edges denote Spearman correlations satisfying |rho| > 0.6 and FDR < 0.05; orange and blue edges indicate positive and negative associations, respectively. Node size is proportional to mean relative abundance. Red, FBDS-enriched candidate genus; blue, FBHS-enriched candidate genera; grey, other dominant genera. Only candidate genera and selected dominant taxa are labelled. Forty-five of 50 input nodes formed at least one edge, yielding 189 edges (189 positive, 0 negative) and a density of 0.154. (C) Network of the FBHS group, constructed under identical parameters. Forty-four of 50 input nodes formed at least one edge, yielding 281 edges (248 positive, 33 negative) and a density of 0.229

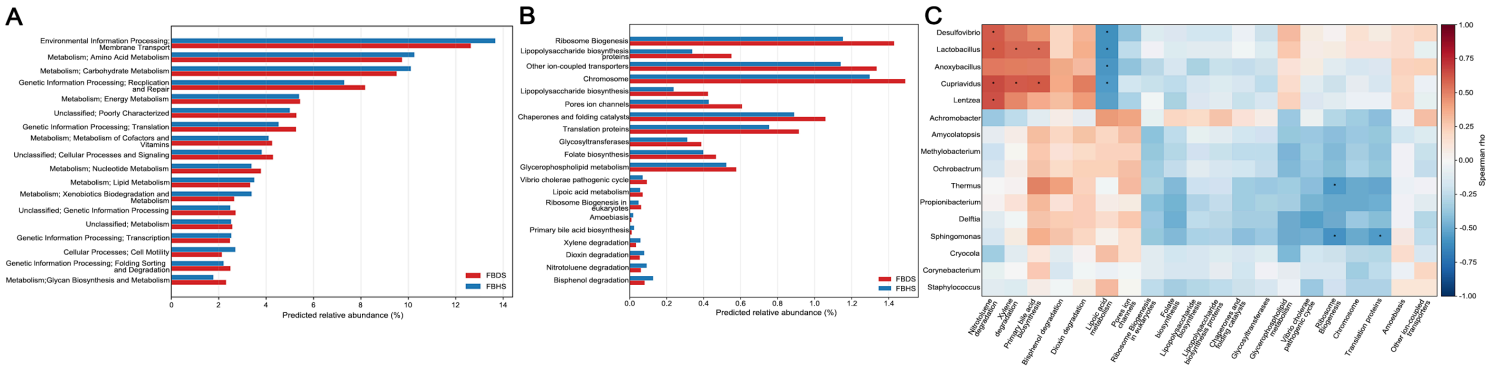


Figure 4

Predicted functional profiles and genus-pathway associations in paired FBDS and FBHS samples. (A) Bar plots showing PICRUSt-predicted KEGG level 2 functional categories in FBDS and FBHS samples. (B) Bar plots showing selected PICRUSt-predicted KEGG level 3 pathways. Red bars indicate FBDS, and blue bars indicate FBHS. Values are shown as predicted relative abundance percentages. (C) Spearman correlation heatmap between paired differences in candidate differential genera and paired differences in selected KEGG level 3 pathways.